Inherent sea ice predictability in the rapidly changing Arctic environment of the Community Climate System Model, version 3

**Marika M. Holland · David A. Bailey ·
Steve Vavrus**

Abstract Seasonal predictions of Arctic sea ice have typically been based on statistical regression models or on results from ensemble ice model forecasts driven by historical atmospheric forcing. However, in the rapidly changing Arctic environment, the predictability characteristics of summer ice cover could undergo important transformations. Here global coupled climate model simulations are used to assess the inherent predictability of Arctic sea ice conditions on seasonal to interannual timescales within the Community Climate System Model, version 3. The role of preconditioning of the ice cover versus intrinsic variations in determining sea ice conditions is examined using ensemble experiments initialized in January with identical ice–ocean–terrestrial conditions. Assessing the divergence among the ensemble members reveals that sea ice area exhibits potential predictability during the first summer and for winter conditions after a year. The ice area exhibits little potential predictability during the spring transition season. Comparing experiments initialized with different mean ice conditions indicates that ice area in a thicker sea ice regime generally exhibits higher potential predictability for a longer period of time. In a thinner sea ice regime, winter ice conditions provide little ice area predictive capability after approximately 1 year. In all regimes, ice thickness has high potential predictability for at least 2 years.

M. M. Holland (✉) · D. A. Bailey
National Center for Atmospheric Research,
1850 Table Mesa Drive, Boulder, CO 80305, USA
e-mail: mholland@ucar.edu

S. Vavrus
University of Wisconsin, Madison, USA

1 Introduction

The Arctic environment is undergoing rapid change across the marine, terrestrial, and atmospheric systems (e.g. Serreze et al. 2007; Overland et al. 2004; Stroeve et al. 2007; Francis and Hunter 2007). Perhaps the most dramatic aspect of this change is manifested in the reduction and thinning of the Arctic floating ice cap (Serreze et al. 2007). Near-term forecasts of sea ice conditions provide important information on the marine accessibility of Arctic seas. These serve a number of uses and a number of institutions provide operational forecasts in order to meet these needs.

Many of these forecasting systems use multiple regression models that rely on statistical relationships present in the historical record (e.g. Walsh 1980; Drobot and Maslanik 2002; Drobot et al. 2006; Lindsay et al. 2008). The predictors used in these systems include a mix of information on previous ice (e.g. concentration, albedo, age), ocean (e.g. temperature) and atmospheric (e.g. incoming longwave radiation) conditions. Forecasting techniques that use ensemble simulations from ice–ocean coupled models with prescribed atmospheric forcing from the historical record have also been explored (Zhang et al. 2008a). Additional work has examined the influence of different factors for an extreme September sea ice anomaly using an adjoint of an ice–ocean coupled model (Kauker et al. 2009), and found that the winter/spring ice thickness and summer wind and air temperature variations played a particularly important role.

Recently, the Study of Environmental Arctic Change (SEARCH) program has requested end-of-summer sea ice "outlooks" from the scientific community in an effort to better assess the methods used to provide short-term forecasts of sea ice conditions. These are focused on the expected September sea ice extent minimum at lead times

of from 1 to 4 months (although investigators often base their outlooks on the previous spring, winter or summer conditions). Information from the official website (http://www.arcus.org/search/seaiceoutlook/index.php) indicates that there are many methods being explored in these outlooks and that these provide considerably different quantitative forecasts.

The various methods documented in these studies do show some skill in forecasting the summer ice cover at a variety of lead-times. However, in the presence of the rapidly changing Arctic environment, statistical relationships used in these forecasting methods (or diagnosed from an ocean–ice coupled model adjoint; Kauker et al. 2009) may not remain valid. Additionally, using prescribed historical atmospheric forcing in ensemble ice–ocean numerical model forecasts neglects feedbacks to the atmosphere. This has important implications for the forecasts, which may be dependent on the mean climate state. To date, limited work has been done to explore the inherent predictability of Arctic sea ice cover. Regional climate modeling experiments focused on the 1980s and 1990s have elucidated aspects of Arctic ice and near-surface climate predictability and the role of regional versus large-scale atmospheric circulation for interannual Arctic climate variability (Döscher et al. 2009). Additionally, Koenigk and Mikolajewicz (2008) have assessed high latitude climate predictability using ensemble experiments with a global coupled climate model and found that central Arctic ice thickness is highly predictable for up to 2 years due to persistence. In contrast, the inherent predictability of sea ice concentration was very low. These simulations used control conditions without rising greenhouse gases and hence did not assess changing aspects of predictability in a changing Arctic environment.

Climate model integrations of the twentieth and twenty-first centuries have been performed with a number of different modeling systems (IPCC 2007). While these models vary in the quality of their Arctic simulations (Zhang and Walsh 2006; Arzel et al. 2006; Gerdes and Koberle 2007; Holland et al. 2008a), they do provide a useful tool to assess changing aspects of Arctic sea ice predictability. Through the use of "perfect initialization" experiments in which multiple ensemble integrations are initialized with identical ice, ocean and terrestrial conditions, we can assess the inherent predictability in the sea ice system within the climate model context. Obtaining initial conditions from different time periods of standard twentieth to twenty-first century integrations allows us to test how predictability characteristics change with the changing climate state.

Here we assess a set of "perfect initialization" ensemble integrations from the Community Climate System Model, version 3 (CCSM3; Collins et al. 2006a) to address a number of interrelated questions regarding sea ice

predictability on seasonal to interannual timescales. In particular, within the climate model system, we assess: (1) What is the inherent predictability of Arctic sea ice? (2) How important is "preconditioning" versus intrinsic variability for subsequent ice conditions? and (3) Do predictability characteristics change with a changing ice state? We assess the predictive capability for both Arctic sea ice thickness and area, with a particular focus on end-of-summer (September) sea ice cover since this has been the subject of a number of recent studies (Drobot et al. 2006; SEARCH outlook activity).

2 Climate model integrations

Climate model integrations from the fully coupled Community Climate System Model, version 3 (CCSM3) are examined. This model includes atmosphere, ocean, land and sea ice components (Collins et al. 2006a). For the integrations considered here, the atmosphere model (CAM3) (Collins et al. 2006b) is run at T85 resolution (approximately 1.4 degrees) with 26 vertical levels. The ocean model (Smith and Gent 2004) includes an isopycnal transport parameterization (Gent and McWilliams 1990) and a surface boundary layer formulation following Large et al. (1994). The dynamic-thermodynamic sea ice model (Briegleb et al. 2004; Holland et al. 2006b) uses the elastic-viscous-plastic rheology (Hunke and Dukowicz 1997), a sub-gridscale ice thickness distribution (Thorndike et al. 1975; Lipscomb 2001) and the thermodynamics of Bitz and Lipscomb (1999). Both the ice and ocean models use a nominally 1-degree resolution grid in which the north pole is displaced into Greenland. The grid spacing over the Arctic Ocean varies from about 20 km · 60 km near Greenland to 50 km · 70 km in the East Siberian Seas. As such, the Arctic Ocean is reasonably well resolved and there is an open channel within the Canadian Arctic Archipelago. The land component (Bonan et al. 2002) includes a subgrid mosaic of plant functional types and land cover types based on satellite observations. It uses the same spatial grid as the atmospheric model.

Previous studies have identified that CCSM3 simulates a reasonable Arctic sea ice climatology in the late twentieth century compared to observations (e.g. Holland et al. 2006a; Gerdes and Koberle 2007). This includes a realistic mean and spatial distribution of Arctic ice thickness and reasonable ice mass budget terms (Holland et al. 2008a), although the Fram Strait ice volume transport is about 50% higher than observed (Holland et al., 2006b). The summer ice extent is very well simulated compared to satellite observations (Fig. 1a). Additionally, CCSM3 is one of only two CMIP3 models with September ice extent trends over the latter part of the twentieth century that are consistent
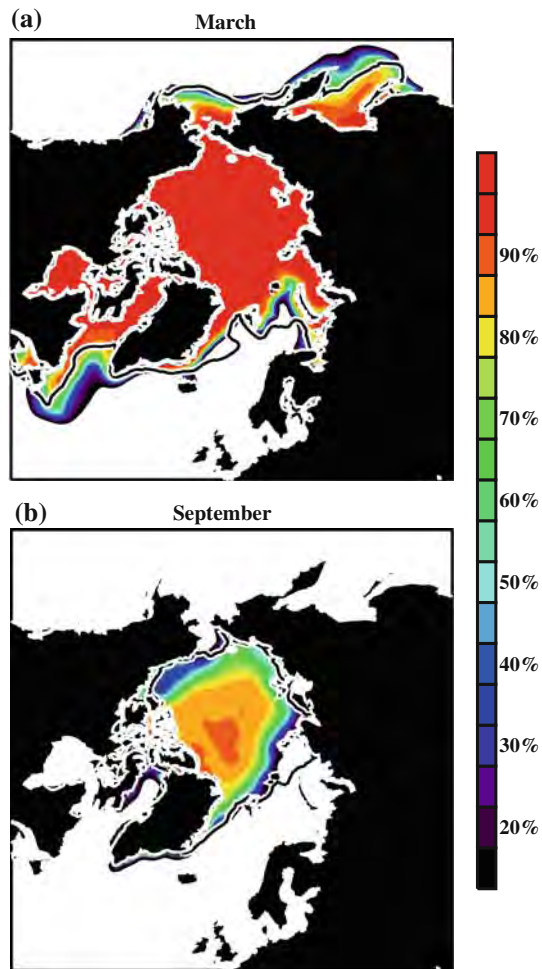
(a) **March**

(b) **September**

Fig. 1 The mean CCSM3 sea ice concentration from 1980 to 1999 for (**a**) March and (**b**) September. The observed ice extent (15% ice concentration contour) is shown by the solid black line

Table 1 A description of the three sets of perfect initialization ensemble integrations

	Initial conditions		Initialization run	Number of members
	Year	Ice thickness		
Set 1	1970	3.2	B30.030a	20
Set 2	2016	1.8	B30.040b	23
Set 3	2017	1.5	B30.040b	20

conditions because restart datasets that are needed to initialize the model were only saved from the existing twentieth to twenty-first century standard model integrations once a year on January 1. The initial atmospheric state varies across the different ensemble members and is obtained from January 1 conditions from different years of the same standard twentieth or twenty-first century CCSM3 integration that was used for the initial ocean–sea ice–terrestrial state. The years used to obtain the atmospheric initial conditions are from the same decade in which the initial ice–ocean–land conditions are chosen (and hence have a similar "climate"), allowing for eleven different possible initial atmospheric states. The ensemble size is increased further by running the simulations on two different computer platforms, which introduces round-off level numeric changes to the runs. This allows for a maximum of 22 ensemble members. Because of computational limitations, from this maximum of 22 members, a subset of 20 integrations were run for the first and third ensemble set. For the second ensemble set, 23 members were run, with the additional member obtained by applying round-off level changes to one of the initial atmospheric states. Given the rapid adjustment time-scales of the atmosphere, which equilibrates to the surface ice–ocean–land conditions within several months (Deser et al. 2007), we expect any inherent predictability in the system on seasonal to interannual timescales to reside in the ocean and/or sea ice initial state. Indeed, the spread across the ensemble members initialized with the same atmospheric state but with round-off level changes introduced is not generally smaller than the spread across ensemble members initialized with different initial atmospheric states. This supports our argument that the initial atmospheric state does not unduly determine the sea ice simulation on monthly-interannual timescales.

The first ensemble set, with 20 members, is initialized with conditions from year 1970 of a standard twentieth century integration (Meehl et al. 2006). This is a relatively thick Arctic sea ice regime (Fig. 2a) similar to observed conditions in the 1960s–1970s (e.g. Bourke and Garrett 1987). In the second and third ensemble sets, with 23 and 20 members, respectively, the initial ice and ocean state were chosen to reflect conditions similar to those of the
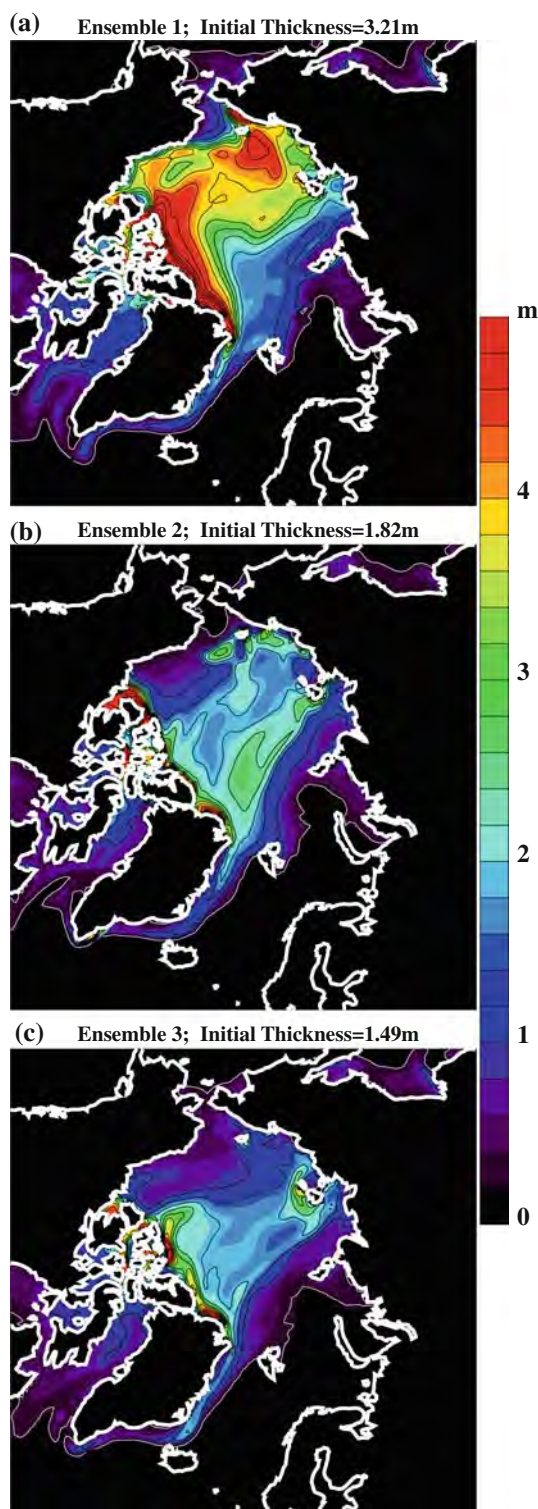
with the observed satellite era ice loss (Stroeve et al. 2007). This suggests that an analysis of predictability characteristics of CCSM3 September ice cover in the twentieth and twenty-first centuries will provide useful information on changing predictability in an Arctic environment under transformation. The simulated winter ice edge (Fig. 1b) also agrees well with observations except in the Labrador Sea where excessive ice cover is associated with low ocean heat transport into that region (Jochum et al. 2008). This may influence winter predictability characteristics diagnosed there.

In order to assess the inherent predictability in Arctic sea ice conditions on seasonal to interannual timescales, we have run three sets of integrations initialized on January 1 and integrated for 2 years (Table 1). The set of "perfect-initialization" ensemble simulations apply identical ocean, sea ice, and terrestrial initial conditions that are obtained from standard twentieth or twenty-first century CCSM3 simulations. We were limited in the timing of the initial

(a) Ensemble 1; Initial Thickness=3.21m

(b) Ensemble 2; Initial Thickness=1.82m

(c) Ensemble 3; Initial Thickness=1.49m

Fig. 2 The January 1 initial ice thickness conditions prescribed for the three different ensemble sets
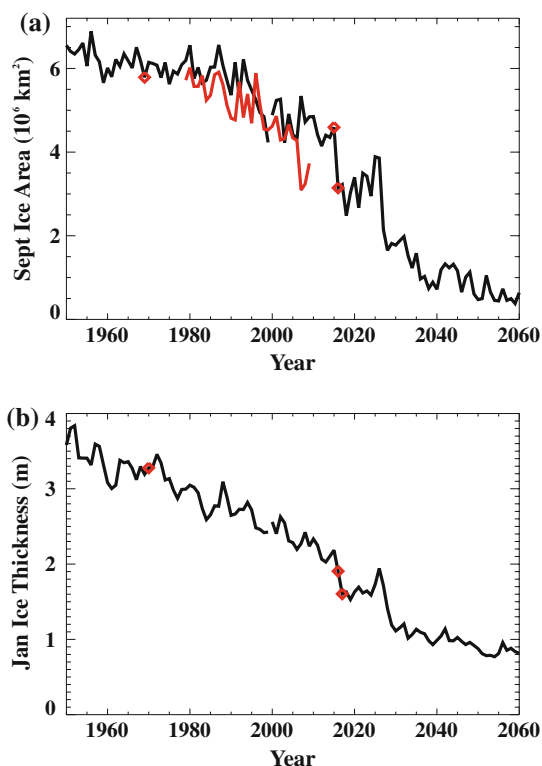
(a)

(b)

Fig. 3 The (**a**) northern hemisphere September ice area and (**b**) Arctic averaged January ice thickness from the twentieth to twenty-first century control run that is used to obtain initial conditions for the ensemble experiments. The *red diamonds* show the years from which the initial conditions are obtained (in panel **a**, these are shown for the time 3 months prior to the January initialization). The *red line* in panel (**a**) shows the observed timeseries of September ice area (Fetterer et al. 2002, updated)

(SRES A1B; IPCC 2007). The specific years used for the initialization of Sets 2 and 3 were chosen based on the control simulation behavior. They differ in that set 2 is initialized with the January 1 conditions just preceding a large reduction in September ice area (of 1.45 million km^2), and set 3 is initialized with the January 1 conditions just following this large ice area loss (Fig. 3). Although much more extreme low-ice states occur later in the simulated twenty-first century, these initial conditions were chosen because they can provide insight into the predictability of large ice loss events similar to that of September 2007 and the conditions following such an event.

The control integrations from which the initial conditions are obtained can be considered another member of the predictability ensembles as they have identical initial ice–ocean–terrestrial conditions for the years in question and they are treated as such for our results in Sect. 3. Different standard CCSM3 ensemble runs were used for the selected twentieth century (1970) initial conditions and twenty-first century (2016 and 2017) initial conditions. This was due to the initial condition availability from these runs. However,

recent historical record with a thinner mean ice pack (Fig. 2b, c). These are obtained from the January 1 conditions from years 2016 and 2017 of a standard twenty-first century integration with a middle range emissions scenario

the standard CCSM3 twentieth to twenty-first century ensemble members are subject to the same timeseries of external forcing (e.g. changing atmospheric greenhouse gas concentrations, volcanic forcing, and solar variability at the top-of-atmosphere) and only differ slightly in their initial preindustrial (year = 1870) state. All of these integrations exhibit long-term declines in Arctic sea ice thickness and area (Holland et al. 2006). Differences across the various ensemble members reflect the contribution of simulated natural variability in the system and as such the initial states chosen for the predictability ensemble experiments represent valid CCSM3 conditions for the respective time periods.

3 Results

Since the ensemble simulations apply an identical initial ice–ocean–terrestrial state (perfect initial conditions) and an identical model (perfect forecast model), the results give a measure of the maximum possible predictability in the system on seasonal-interannual timescales. The three different sets of ensemble members (Table 1), with different initial conditions (Fig. 2), allow us to explore the importance of the changing mean sea ice state for the seasonal-interannual predictability characteristics. Set 1 has relatively thick sea ice, whereas Sets 2 and 3 have thinner conditions more similar to the recently observed state (e.g. Stroeve et al. 2008).

The timeseries of northern hemisphere September ice area and January Arctic basin averaged ice thickness for 1950–2060 from the control integrations that are used to obtain initial conditions in the ensemble sets are shown in Fig. 3. These standard twentieth to twenty-first century simulations, including the Arctic sea ice conditions, have been assessed previously (e.g. Holland et al. 2006a; Meehl et al. 2006) and were discussed in the IPCC-AR4 (IPCC 2007). Similar to observations and hindcast simulations forced with atmospheric data (e.g. Maslanik et al. 2007; Rothrock et al. 2003), the simulated ice volume shows a considerable decline over the late twentieth to early twenty-first century in all of the CCSM3 standard runs with a corresponding reduction in the summer sea ice area. As discussed by Stroeve et al. (2007), the reduction in September ice extent in these simulations is consistent with observed sea ice loss over the satellite record.
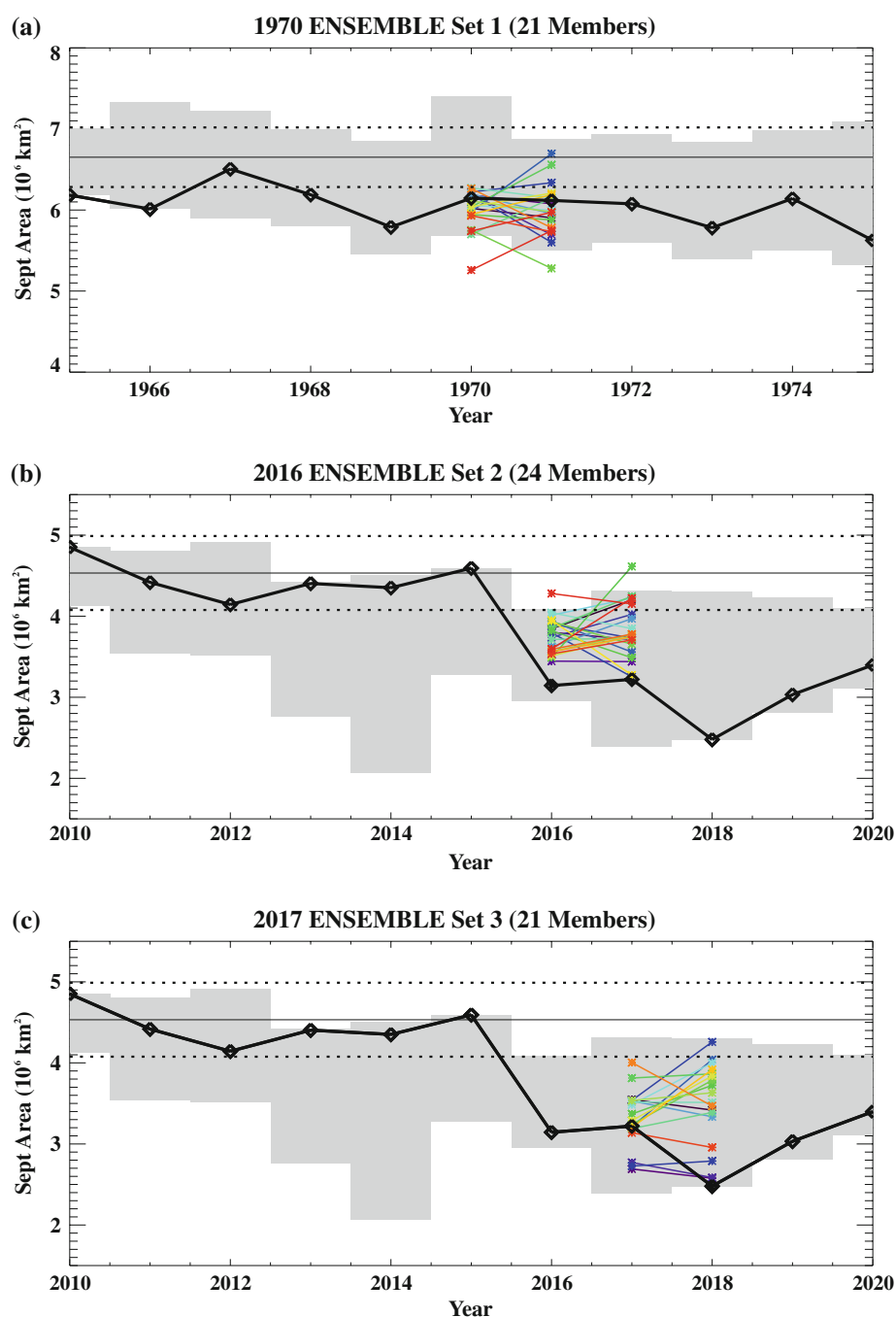
3.1 Ensemble integrations

Here we assess the predictability characteristics of the Arctic ice area. Analysis using ice extent (defined as the region with greater than 15% ice cover), which is commonly used in observational studies, shows the same qualitative behavior. September ice area for the three sets of perfect initialization ensemble simulations with a comparison to the eight member ensemble of the standard twentieth to twenty-first century integrations is shown in Fig. 4. In all three of the perfect initialization ensemble sets, there is a considerable spread in the September sea ice area simulated 9 months into the integrations. The standard deviation in the September ice area across the ensemble members is lowest for the late twentieth century ensemble set and generally increases for the ensemble sets with thinner ice cover, especially Ensemble Set 3 (Table 2) for which the difference in variance is statistically significant (at the 95% level) for the September values of Year 2. An increase in variance with a thinning ice pack is consistent with previous studies on Arctic sea ice variability (Holland et al. 2008b; Goosse et al. 2009), and is reflected in the larger range across the standard twentieth to twenty-first century ensemble integrations shown by the grey shading.

From the 1979–2008 satellite observations, the year-to-year changes in September ice area have a significant negative 1-year lagged autocorrelation ($R = -0.59$) meaning that an increase in September ice cover is typically followed by a decrease in ice cover the next year. This occurs even with the large downward trend in September sea ice over this time period because the one-year reductions in ice are considerably larger than the recovery that often occurs the next year. A similar lagged autocorrelation behavior is seen in the members from Ensemble Sets 1 and 2 (Table 2), where the September ice area change in Year 1 and Year 2 are significantly correlated at -0.50 and -0.46, respectively. For Ensemble Set 3, the correlation is not significant at -0.05. The observed and simulated negative correlation is likely related to negative feedbacks, such as the fact that thinner ice cover grows more rapidly subject to the same forcing. This fundamental aspect of sea ice thermodynamics gives rise to a negative feedback with a stabilizing influence on sea ice conditions (Bitz and Roe 2004). The low correlation in Ensemble Set 3 suggests that the influence of these stabilizing feedbacks is overwhelmed by other factors such as the inherent variability of the system and positive feedbacks such as that due to surface albedo changes. The standard deviation in September ice area increases for the second year of integration with the increase being largest for Set 3. This suggests that there is some "knowledge" of the initial conditions during the first September of integration, which decreases the following year. The stabilizing feedback implicit in the ice area change correlation should counteract this but is not strong enough to overcome it.

While the spread among the ensemble members is large, there are some similar features within each ensemble set. For example, when compared to September conditions in the control run several months prior to initialization, many

Fig. 4 The timeseries of September ice area for the three ensemble sets. The *black line* shows the control simulation from which the ensemble member initial conditions were obtained; the *colored lines* show the ensemble member simulations; and the *grey shading* shows the range across the eight standard CCSM3 integrations of the twentieth or twenty-first century. The *thin solid* and *dotted black lines* show the mean and plus/minus one standard deviation from the multi-century preindustrial (panel **a**) and present-day (panels **b** and **c**) control integrations

of the ensemble members exhibit a change in ice area of a similar sign (Table 2). This is especially true of Ensemble Set 2, in which the initial conditions were chosen just prior to a large September ice loss in the standard CCSM3 control integration. In this ensemble set, all 23 of the members exhibit a reduction in September ice area compared to the September area of 4.6 million km² that was simulated in the control run several months prior to initialization. Indeed all but one of the ensemble members simulates a September ice area lower than anything in the previous decade of the control integration. This suggests

that preconditioning of the ice cover, as represented by the identical January initial conditions in all of the ensemble members, plays an important role for the resulting ice area reduction. Indeed, the January ice thickness used to initialize the Set 2 integrations is anomalously thin in the Beaufort/Chukchi/East Siberian Sea region compared to the standard twenty-first century CCSM3 integrations for a comparable time period (not shown). It is also notable that for this ensemble set none of the other ensemble members has an extreme reduction in ice area of the same magnitude as the standard twenty-first century scenario run from

Table 2 Statistics for the September ice characteristics from the different ensemble sets, including the standard deviation of ice area across the ensemble members, the autocorrelation of the change in September area from one year to the next for year 1 and for year 2, and the fraction of ensemble members that exhibit an increase in September ice area in year 1 compared to the September conditions obtained just prior to the ensemble set initialization

	Standard dev		$R(\Delta yr1, \Delta yr2)$	Fraction that increase in Year 1
	Year 1	Year 2		
Set 1	0.241	0.319	−0.50	0.80
Set 2	0.243	0.351	−0.46	0.0
Set 3	0.341	0.538	−0.05	0.75

which the initial conditions were obtained (Fig. 5). This suggests that although preconditioning in the form of an anomalously thin winter ice pack may be necessary to initiate a large ice area loss, it is not sufficient to initiate that loss. Instead, it must be reinforced by sizable intrinsic variations in the spring and summer atmosphere and/or ocean conditions, which appear to be quite rare. This is broadly similar to conclusions on the contributing factors of the large ice loss in September of 2007 (Stroeve et al. 2008; Kay et al. 2008; Schweiger et al. 2008; Zhang et al. 2008b; Lindsay et al. 2009). In particular, the adjoint analysis of Kauker et al. (2009) showed that the initial (March) ice thickness in combination with May–June wind conditions, and September air temperature explained nearly 90% of the 2007 September sea ice area anomaly (Kauker et al. 2009).

Over time, the perfect initialization ensemble members diverge due to the chaotic nature of the system. The spread
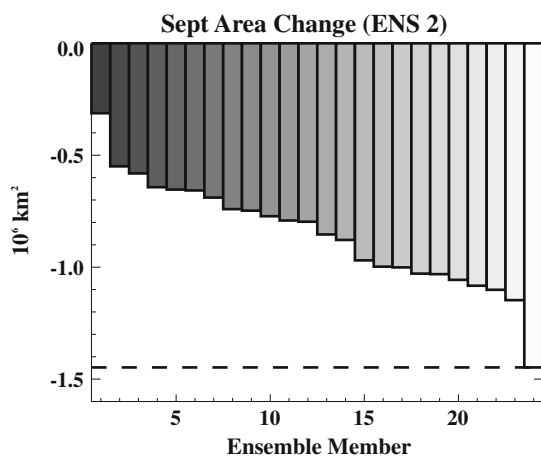

Fig. 5 The September ice area change in Year 1 for the 23 members of ensemble set 2. The difference is taken relative to the September ice area in the control integration that occurred prior to the ensemble set initialization. The area change in the twenty-first century control integration that provides the initial conditions for Ensemble Set 2 is shown by the final ensemble member and the *dashed line*

in sea ice conditions across the ensemble members results from variations in dynamic and thermodynamic sources and sinks of sea ice. The resulting changes in these terms (i.e. changes in ice melt, growth and divergence) directly influence the ice thickness and indirectly modify ice area when, for example, entire regions of the ice cover melt out in summer. During model run time, the monthly change in ice volume at each model grid cell that results from thermodynamic processes and from dynamic processes is separately diagnosed. Similar diagnostics are computed for the change in ice area that results from thermodynamic and dynamic processes. An analysis of these terms allows us to separate the influence of thermodynamic change versus dynamic change for the evolving sea ice conditions. The thermodynamic processes include all growth and melt terms, including frazil and basal ice formation, snow-to-ice conversion, and surface, basal, and lateral melting. The dynamic processes include ice divergence due to transport and, in the case of ice area change, ridging and rafting processes that reduce ice area while conserving ice volume.

A diagnosis of how variations in these sea ice mass budget terms contribute to the scatter in September ice area across ensemble members provides insight on the role of intrinsic forcing variability for potential sea ice predictability. We show, for each ensemble set, the correlation across ensemble members of the Year 1 September sea ice area and the Arctic basin average change in ice volume (Fig. 6) and ice area (Fig. 7) since initialization. This is computed separately for the ice volume and area changes resulting from dynamic and thermodynamic processes. Put another way, for each month of simulation (shown on the x-axis) the total change in ice volume since initialization due to thermodynamic processes is correlated with the following September ice area (Fig. 6a). This is similarly done for ice volume change due to dynamic processes (Fig. 6b) and for thermodynamically and dynamically driven ice area change (Fig. 7a, b). Correlations are computed separately for each ensemble set.

For all of the ensemble sets, the scatter across the ensemble members in the summer thermodynamic (i.e. melt) driven ice volume change (Fig. 6a) is significantly correlated to the following September ice area. This indicates that differences in summer ice melt, and the consequent ice thickness, are largely responsible for the spread in September ice area in the different ensemble members. In contrast, scatter in the dynamic driven anomalies in ice volume (i.e. ice export; Fig. 6b) generally show smaller correlations with the subsequent September ice area. Indeed, significant correlations only occur for ensemble Set 3 during the summer months and ensemble Set 1 during September; these are considerably smaller than the correlations with thermodynamically driven ice volume changes.
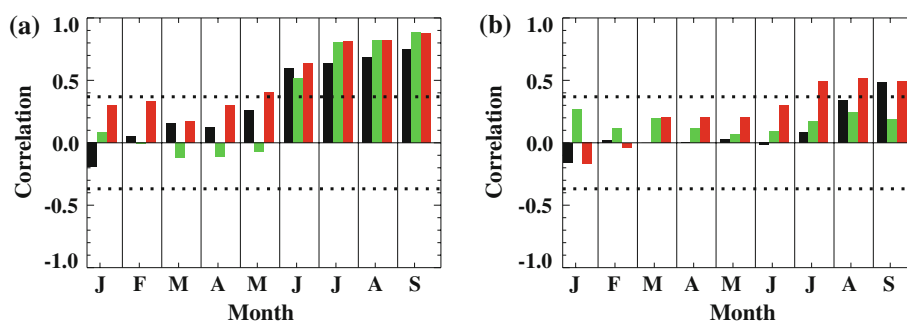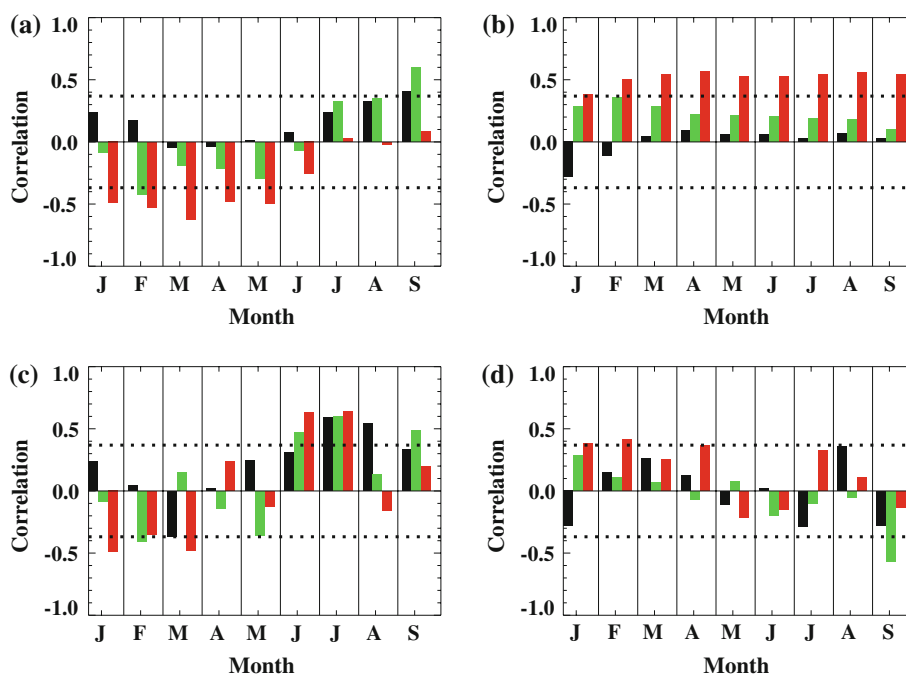
Fig. 6 The correlation across the ensemble members of the total change in Arctic averaged ice volume since initialization with the following September ice area. Shown are the correlations of September area with (**a**) the total ice volume change resulting from thermodynamic processes, (**b**) the total ice volume change resulting from dynamic processes. Ensemble Set 1 is in *black*, Ensemble Set 2 in *green* and Ensemble Set 3 in *red*. The *dashed line* indicates the 95% statistical significance threshold

Fig. 7 The correlation across the ensemble members of the change in Arctic ice area over time with the following September ice area. Shown are the correlations of September area with (**a**) the total ice area change since initialization resulting from thermodynamic processes, (**b**) the total ice area change since initialization resulting from dynamic processes, (**c**) the monthly ice area change resulting from thermodynamic processes and (**d**) the monthly ice area change resulting from dynamic processes. Ensemble Set 1 is in *black*, Ensemble Set 2 in *green* and Ensemble Set 3 in *red*. The *dashed line* indicates the 95% statistical significance threshold

Differences in the ice volume simulation across the ensemble members affect ice area by influencing the region that can potentially melt out during summer or by modifying the strength of the ice pack and resulting ice motion and convergence. An examination of the relationship between the ice area change terms and subsequent September ice area (Fig. 7) indicates that different mechanisms are important in the different ensemble sets. During winter, dynamic ice area loss in the Arctic resulting from export or convergence is balanced by thermodynamic ice area gain as newly opened water rapidly refreezes. This leads to an almost perfect anti-correlation between the Arctic thermodynamic and dynamic sources of open water during winter (not shown) and causes comparable (but opposite sign) correlations in Fig. 7a,b for January through May. It also allows the Arctic Ocean to remain almost

completely ice covered through April in all of the ensemble sets.

The dynamic and thermodynamic ice area change no longer balance over the melt season, resulting in a reduction in ice area. During this time period, it is illustrative to consider the ice area changes during each month (Fig. 7c, d), as opposed to the time-integrated changes since initialization (Fig. 7a, b). For all ensemble sets, ice area loss resulting from net melt during the summer plays an important role in the ultimate scatter of September ice cover across the ensemble members (Fig. 7c). The timing of these important melt anomalies differs among the ensemble sets and generally occurs a month earlier in the thinner ice regime (Set 2 and Set 3) where summer melt more readily leads to open water formation. Additionally, the processes that enhance thermodynamic ice area loss

(melt out) in some ensemble members are different across the ensemble sets. All ensemble sets exhibit enhanced summer open water formation for integrations with larger summer ice volume melt. However, ensemble Set 3 also has enhanced melt out (thermodynamic ice area loss) in simulations which have higher dynamic ice area loss during the previous winter. This is reflected in the significant positive correlations (Fig. 7d) found in January and February for Ensemble Set 3. Indeed, in Set 3, the June thermodynamic ice area loss (melt out) is significantly correlated to dynamic ice area loss during winter (at $R = 0.6$; not shown). While any winter dynamic ice area loss quickly freezes over leading to little change in ice area, it does redistribute the ice and modify the ice thickness distribution. In particular, enhanced ridging leads to a broader distribution with a larger area of thin ice, which is then more able to melt out the following summer. This appears to play an important role in Set 3, but not in the other ensemble sets. This is likely related to the thin conditions used for initialization of the Set 3 ensemble members. Since thinner ice is weaker and more able to converge and shear, larger variations in ridging are possible across the Set 3 ensemble members. That different factors determine the resulting scatter in simulated September sea ice conditions for the various ensemble sets, strongly suggests that different ice thickness regimes and extreme events have different predictability characteristics.

3.2 Prognostic potential predictability of sea ice conditions

The potential predictability of the sea ice system can be quantified by diagnosing how quickly the ensemble simulations diverge and comparing this to the natural variability in the system (e.g. Koenigk and Mikolajewicz 2008; Pohlmann et al. 2004). We assess the expected spread due to natural variability using a multi-century present-day integration and a multi-century preindustrial integration of the model. The present-day and preindustrial simulations have fixed external forcings (e.g. greenhouse gas levels, top-of-the-atmosphere solar forcing, etc.) that are consistent with observed conditions for 1990 and 1870 time periods, respectively.

We choose a number of different characterizations of the intrinsic variability because the variability changes with the mean climate state (Fig. 8). In a thinner sea ice regime like the present day control integration, the natural variability in northern hemisphere sea ice area is generally lower in winter and higher in late summer-early autumn. The present-day integration has a similar annual cycle of mean ice area and Arctic thickness to the scenario runs for the 2010–2020 time period, with the monthly mean values generally lying within one standard deviation of each other
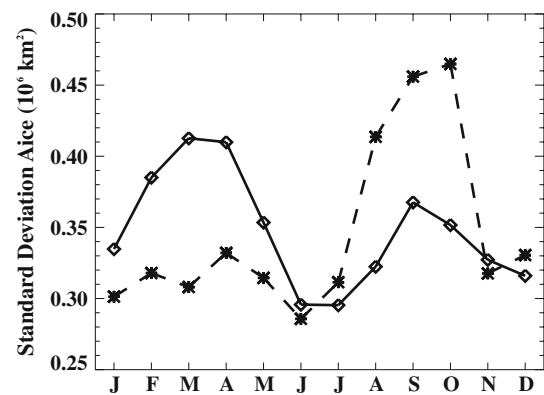

Fig. 8 The standard deviation of northern hemisphere ice area for a present-day (*dash*) and pre-industrial (*solid*) control integration

(not shown). As such, this control integration provides a long timeseries that allows for robust statistics for comparison to Ensemble Sets 2 and 3. The characterization of natural variability for Ensemble Set 1 is more problematic. The preindustrial and present-day control integrations bracket the mean sea ice conditions from this Ensemble Set. As such, we compare this Ensemble Set to the intrinsic variability obtained in both of these control runs, which likely brackets the true intrinsic variability of the climate model for mean sea ice conditions similar to those of Ensemble Set 1.
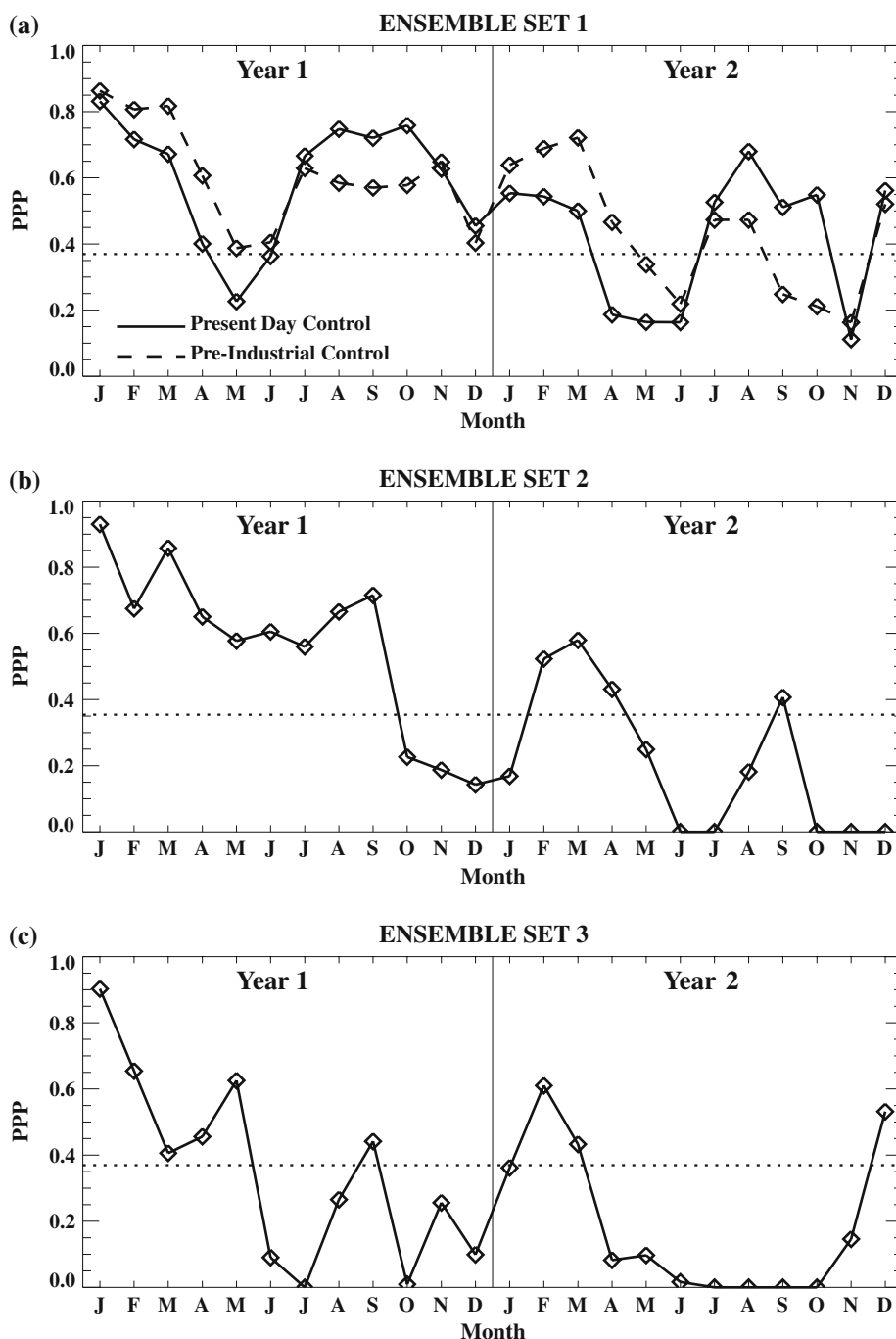
The prognostic potential predictability (PPP) (e.g. Koenigk and Mikolajewicz 2008; Pohlmann et al. 2004) provides a measure of the spread across ensemble experiments compared to the natural variability. It is defined as:

$$\text{PPP}(t) = 1 - \frac{\sigma_e^2}{\sigma_c^2}$$

where σ_e^2 is the variance across the ensemble members at time t and σ_c^2 is the variance of the control integration for the relevant month (Fig. 8). The significance is estimated using an F-test as in Pohlmann et al. (2004). A PPP value of 1 corresponds to a perfectly predictable system (i.e. the ensemble members do not diverge over time), whereas a PPP value of zero implies no predictability because the ensemble spread is equal to that expected from natural variability. While the ensemble spread may not be statistically different than that diagnosed from natural variability, it can in practice be slightly higher than σ_c^2 and lead to negative PPP values. In this case, PPP is defined to be identically zero.

Figure 9 shows the PPP for northern hemisphere ice area for the three different sets of perfect-initialization ensemble simulations at each month of integration. The different ensemble sets have some broadly similar characteristics over the 2 years of integration. All of the ensemble sets show significant potential predictability

Fig. 9 The prognostic potential predictability of northern hemisphere ice area for the three Ensemble Sets. In panel **a**, the prognostic potential predictability is assessed relative to both the present day (*solid*) and pre-industrial (*dash*) control integrations. The *dotted line* indicates the 95% statistical significance threshold

during the first few months (JFM) of integration when they are highly constrained by their respective initial conditions. During the spring transition season (AMJ), the prognostic potential predictability generally drops in all cases, although it remains significant for some months and some ensemble sets. It then rises again during all or part of the summer (JAS), depending on the ensemble set. Additionally, all ensemble sets exhibit significant PPP values during all or part of winter in the second year with following decreases during the second spring of integration.

While the ensemble sets have these general character-istics in common, there are some considerable differences as well. Ensemble Set 1, with relatively thick sea ice conditions, retains significant potential predictability throughout most of the first year of integration and has particularly high values over the summer. It also retains significant potential predictability during all or most of the second summer (depending on the characterization of natural variability used for comparison). Ensemble Set 2 also exhibits significant potential predictability over the

spring and summer of Year 1. After April of the second year, Set 2 has essentially no significant potential predictability except during September of the second year. Ensemble Set 3 generally has the lowest PPP values. It has little significant potential predictability from June through December of Year 1, although September does exhibit marginally significant predictability in the first year. This set has no significant PPP values after March of Year 2 except during the final month of integration.

Taken together, these results suggest that regardless of the sea ice regime, prognostic potential predictability is generally significant for the first and second winters, ice area during the spring transition season shows less predictability, and summer ice area has potential predictability with a 9-month lead time. Much of the significant winter predictability is associated with conditions in the Labrador Sea (not shown), especially in the thick sea ice regime, which is consistent with results from Koenigk and Mikolajewicz (2008). Although it varies somewhat for different ensemble sets, the significant summer predictability during Year 1 is influenced by high predictability within the Barents Sea region (not shown). This differs from Koenigk and Mikolajewicz (2008) who found higher, but not significant, PPP values there. Contrasting the results from the various ensemble sets suggests that a thicker sea ice regime generally exhibits higher prognostic potential predictability in ice area for a longer period of time and summer ice area is potentially predictable for up to 2 years. In the thinner sea ice regime, winter ice conditions generally give less predictive capability for summer ice conditions, especially after a year.

To understand the reasons for the differences in end of summer predictability among the ensemble sets, it is illustrative to consider the location of September sea ice concentration variability across the ensemble members (Fig. 10). As expected, the concentration variability primarily occurs along the ice edge and only small anomalies are present in the thick, perennially ice covered interior region. Thus, for the thick ice ensemble, the variability is in the Arctic shelf regions and confined by the Arctic coast. In the thinner ice regime, the perennial pack is smaller in area. Initializing with conditions preceding and just following the large ice loss event, provides some predictability in the first summer primarily because there is a region along the Alaskan and Siberian (for Ensemble Set 3) coast that melts out in all of the ensemble members. This leads to little ice concentration variance there in Year 1. However, these regions can potentially exhibit rapid ice growth in the following fall and achieve relatively thick ice cover at the initiation of the second year melt season. This can allow them to maintain a thin sea ice cover through the second summer such that during Year 2, in the absence of the identically specified thin preconditioned winter conditions,

these regions do recover sea ice in some ensemble members. This leads to an increase in ice area variance and less predictive potential. In contrast, for the thick ice regime where large scatter in ice concentration across the ensemble members occurs right up to the coast (i.e. some ensemble members retain ice along the coast in September of Year 1), increased ice area variance in year 2 would require melting out some of the thicker interior ice pack for some ensemble members. This is quite difficult because of the thick nature of this ice and the considerable heat that would be required. This suggests that, compared to ice cover, ice thickness is predictable on longer timescales; a point that we return to below.

The winter ice area exhibits potential predictability for a year in all of the Ensemble Sets. As discussed by Bitz et al. (2005), the location of the mean winter ice edge is strongly related to ocean heat flux convergence. It follows, that variations in ocean heat transport are likely important for the winter ice edge variability. Because of relatively long ocean advective timescales this allows for considerable predictability in the winter ice edge after a single year (and potentially much longer, although we can not assess this with our current experiments). This is true across all of the ensemble sets and is not strongly related to the mean Arctic climate state.

In contrast to ice area, the Arctic ice thickness shows significant potential predictive skill for all ensemble sets for almost the entire 24 months of integration (Fig. 11). This agrees with the results from Koenigk and Mikolajewicz (2008) and is also consistent with the lower frequency variability exhibited by ice volume. Interestingly, while ice area shows higher potential predictability in a thick ice regime (Ensemble Set 1), the ice thickness shows lower predictability in this regime. We hypothesize that this is related to the ice thickness-ice growth rate feedback (Bitz and Roe 2004), which has a stabilizing influence and is more effective for thin ice cover.

4 Conclusions and discussion

The inherent predictability of Arctic sea ice in the CCSM3 model on seasonal to interannual timescales has been investigated through the use of perfect initialization ensemble experiments. These simulations are initialized with identical ice–ocean–terrestrial conditions on January 1 and integrated for 2 years. We perform three different such ensemble sets, with different initial conditions, to assess the role of the mean sea ice state on predictability characteristics. The initial conditions are obtained from a standard twentieth to twenty-first century integration and represent the kind of changes in sea ice state that have occurred during the last 30 years. As such, the results from

Fig. 10 The region where ice concentration standard deviation exceeds 15% for the different ensemble sets for September of Year 1 (*left panels*) and Year 2 (*right panels*). Ensemble Set 1 is shown in the *top panels* (**a**, **b**), Set 2 is shown in the *middle panels* (**c**, **d**), and Set 3 is shown in the *bottom panels* (**e**, **f**)
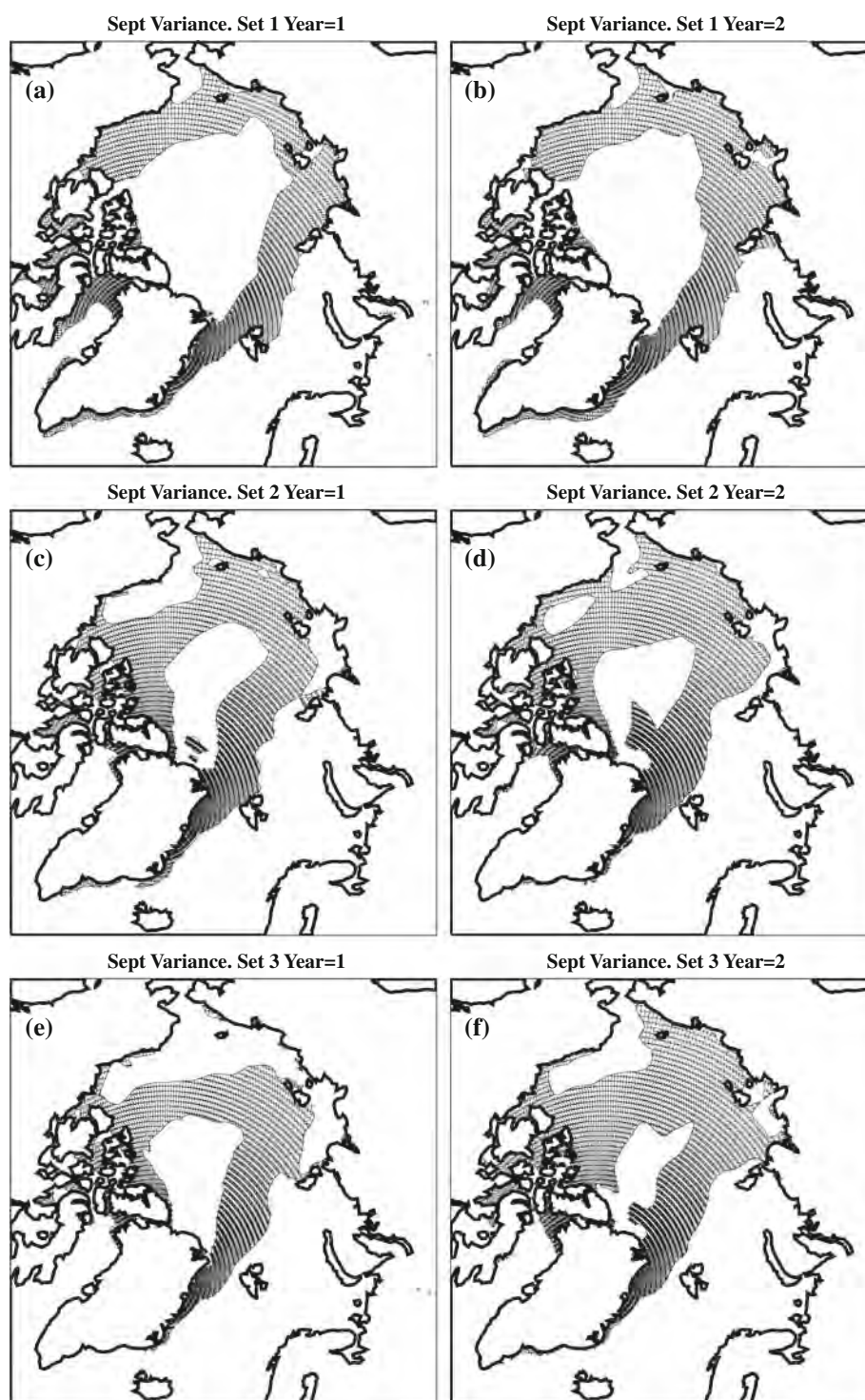

this study provide useful information on the potential forecasting of Arctic sea ice conditions in the rapidly changing Arctic environment that we are currently experiencing.

Our results suggest that, regardless of the initial ice state, the Arctic ice area exhibits potential predictability during the first few months of integration, which then drops during the spring transition season, and rises again during summer. All of the ensemble sets simulate significant prognostic potential predictability of ice area during the first September of integration (although it varies considerably across the ensemble sets and is quite low in Ensemble Set 3). This indicates that winter sea ice preconditioning (i.e. the January sea ice initial state in our

Fig. 11 The prognostic potential predictability of Arctic basin ice thickness for the three Ensemble Sets. For Ensemble Set 1 (panel **a**), the prognostic potential predictability is assessed relative to the present day (*black*) and pre-industrial (*red*) control integrations. The *dotted line* indicates the 95% statistical significance threshold
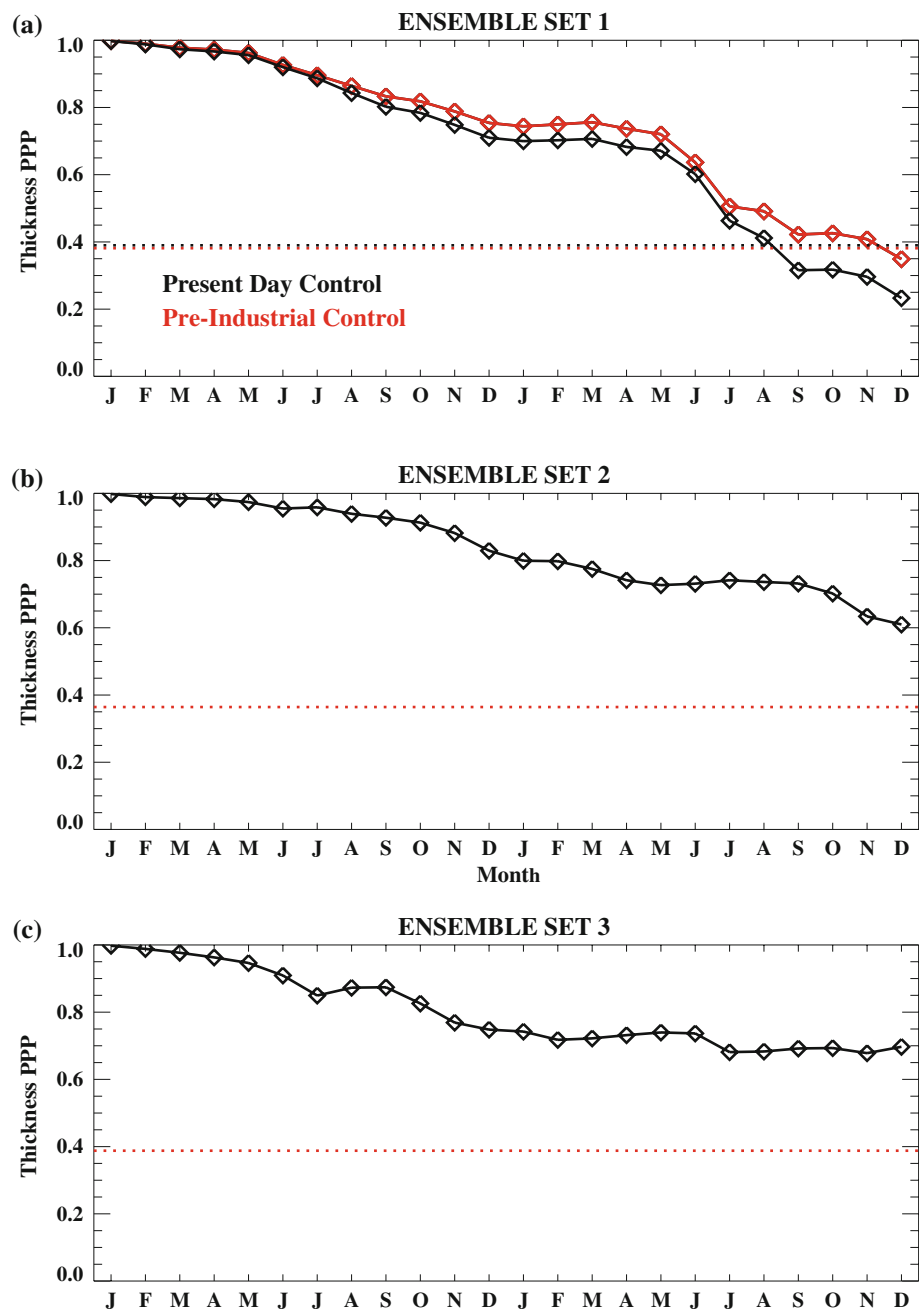
experiments) provides some summer ice area predictive capability, which is consistent with ice–ocean coupled model studies (Kauker et al. 2009). As such, efforts should be made to better observe the Arctic ice thickness distribution, a conclusion also arrived at by the SEARCH Outlook effort.

A correlation analysis reveals that limits on the predictability of September sea ice area are primarily related to intrinsic variations in the thermodynamic-driven ice volume (i.e. melt/growth) anomalies that then translate into different amounts of open water formation over the melt season. Summer (JJAS) melt variations are particularly

effective at driving scatter across the ensemble members, although for some ensemble sets, winter ice growth anomalies also play a role. Dynamic driven ice volume and ice area anomalies have generally a smaller influence on reducing the September ice extent predictability, except in Ensemble Set 3. In Ensemble Set 3 integrations, which are initialized with thin sea ice following a large summer ice-loss event, there is evidence that variations in the amount of ridging among the ensemble members in spring are important for redistributing the ice cover, allowing larger variations in summer melt-out and affecting the end-of-summer scatter in ice area.

During the second year of integration, all of the ensemble members exhibit potential predictability for the winter sea ice conditions. We speculate that this is related to the role of the ocean (with intrinsically long-timescales) in determining the winter ice edge. For the remainder of Year 2, Ensemble Sets 2 and 3 exhibit little potential ice area predictability. In contrast, Ensemble Set 1 exhibits significant prognostic potential predictability during the second summer of integration. Indeed, the potential predictability is generally higher in this ensemble set throughout the 2 years of integration. This set is initialized with thick ice conditions obtained from 1970 of the CCSM3 twentieth century integration; whereas the other sets are initialized with sea ice conditions more consistent with the current observed Arctic conditions. Thus, while one might expect that the summer Arctic sea ice is becoming more predictable due to the strong downward trend, our results suggest that on seasonal to interannual timescales the opposite is true. Ice area is more predictable in a thick sea ice regime and future summer ice area will be harder to forecast with continued thinning of the pack ice. Additionally from a comparison of Ensemble Set 2 and Set 3, which are initialized just preceding and just following a large 2007-like summer ice loss event, we find that even one year changes in the January ice thickness used for initialization (albeit large changes in this case) modify the predictability characteristics, with thinner initial ice conditions (Ensemble Set 3) generally resulting in less predictive capability.

The difference in summer predictability in different sea ice regimes appears in many respects to be a simple matter of geography. The summer ice concentration variability is concentrated along the ice edge with little variability present in the thicker interior ice pack. For a thick ice regime, such as Ensemble Set 1, this variability occurs along the shelf regions and is confined by the coast. In the thinner ice regimes prescribed as the initial conditions in Ensemble Sets 2 and 3, there is a region along the shelf that melts out in the first summer of all the ensemble members with consequently little variability there. In the following year, these regions are able to retain sea ice in some integrations leading to higher variability across the ensemble members and less inherent predictability.

Our results have implications for the design of sea ice forecasting systems. In particular, they suggest that historically based observational relationships used in statistical regression models may have less relevance in future (or possible present) sea ice regimes. This indicates that physically based models may have greater utility in future sea ice forecasting systems. While several ice–ocean coupled modeling systems have been used in the SEARCH Outlook effort, the lack of feedbacks to the atmospheric state is a concern that requires further investigation.

Regional coupled climate modeling systems that include these feedbacks (e.g. Döscher et al. 2009) may provide an alternative forecasting tool although issues still arise on whether they can be adequately initialized. Regardless, our results do suggest that for all sea ice regimes, the intrinsic atmospheric variability during summer months places a strong limit on the predictability resulting from winter sea ice/ocean conditions.

We have only examined simulations initialized on January 1 for this study, which was necessitated by the data availability. However, a number of existing seasonal prediction systems forecast end of summer sea ice cover using springtime information. It is unclear what the potential predictability of sea ice conditions is given a smaller lead time. Since our integrations indicate that summertime thermodynamic forcing was an important factor in reducing the inherent predictability of end-of-summer ice cover, it is not clear that a smaller lead time (e.g. initializing with March conditions) will provide a greatly enhanced potential predictability. Additionally, this study only assessed integrations from a single coupled model and issues such as model biases and model resolution may influence the simulated predictability characteristics. These issues will be explored further in future work.

References

Arzel O, Fichefet T, Goosse H (2006) Sea ice evolution over the 20th and 21st centuries as simulated by current AOGCMs. Ocean Model 12:401–415

Bitz CM, Roe GH (2004) A mechanism for the high rate of sea-ice thinning in the Arctic Ocean. J Clim 17:3622–3631

Bitz CM, Holland MM, Hunke E, Moritz RE (2005) Maintenance of the sea-ice edge. J Clim 18:2903–2921

Bonan GB et al (2002) The land surface climatology of the Community Land Model coupled to the NCAR Community Climate Model. J Clim 15:3123

Bourke RH, Garrett RP (1987) Sea ice thickness distribution in the Arctic Ocean. Cold Reg Sci Tech 13:259–280

Briegleb BP, Bitz CM, Hunke EC, Lipscomb WH, Holland MM, Schramm JL, Moritz RE (2004) Scientific description of the sea ice component in the Community Climate System Model, version 3. NCAR Tech Note. NCAAR/TN-463+STR

Collins WD et al (2006a) The Community Climate System Model: CCSM3. J Clim 19:2122–2143

Collins WD et al (2006b) The formulation and atmospheric simulation of the Community Atmospheric Model: CAM3. J Clim 19:2144–2161

Deser C, Tomas RA, Peng S (2007) The transient atmospheric circulation response to north Atlantic SST and sea ice anomalies. J Clim 20:4751–4767. doi:10.1175/JCLI4278.1

Döscher R, Wyser K, Meier HEM, Qian M, Redler R (2009) Quantifying Arctic contributions to climate predictability in a regional coupled ocean-ice-atmosphere model. Clim Dyn. doi:10.1007/s00382-009-0567-y

Drobot SD, Maslanik JA (2002) A practical method for long-range forecasting of ice severity in the Beaufort Sea. Geophys Res Lett 29(8):1213. doi:10.1029/2001GL014173

Drobot SD, Maslanik JA, Fowler C (2006) A long-range forecast of Arctic summer sea-ice minimum extent. Geophys Res Lett 33. doi:10.1029/2006GL026216

Fetterer F, Knowles K, Meier W, Savoie M (2002) Updated 2007: sea ice index. National Snow and Ice Data Center, Boulder. Digital media

Francis JA, Hunter E (2007) Changes in the fabric of the Arctic's greenhouse blanket. Environ Res Lett 2. doi:10.1088/1748-9326/2/4/045011

Gent PR, McWilliams JC (1990) Isopycnal mixing in ocean circulation models. J Phys Oceanogr 20:150–155

Gerdes R, Koberle C (2007) Comparison of Arctic sea ice thickness variability in IPCC climate of the 20th century experiments and in ocean-sea ice hindcasts. J Geophys Res 112:C04S13. doi:10.1029/2006JC003616

Goosse H, Arzel O, Bitz CM, de Montety A, Vancoppenolle M (2009) Increased variability of the Arctic summer ice extent in a warmer climate. Geophys Res Lett 36:L23702. doi:10.1029/2009GL040546

Holland MM, Bitz CM, Tremblay B (2006a) Future abrupt reductions in the Summer Arctic sea ice. Geophys Res Lett 33:L23503. doi:10.1029/2006GL028024

Holland MM, Bitz CM, Hunke EC, Lipscomb WH, Schramm JL (2006b) Influence of the sea ice thickness distribution on Polar Climate in CCSM3. J Clim 19:2398–2414

Holland MM, Serreze MC, Stroeve J (2008a) The sea ice mass budget of the Arctic and its future change as simulated by coupled climate models. Clim Dyn. doi:10.1007/s00382-008-0493-4

Holland MM, Bitz CM, Tremblay B, Bailey DA (2008b) The role of natural versus forced change in future rapid summer Arctic ice loss. In: DeWeaver ET, Bitz CM, Tremblay L-B (eds) Arctic sea ice decline: observations, projections, mechanisms, and implications. Geophys Monogr Ser, vol 180. AGU, Washington, pp 133–150

Hunke EC, Dukowicz JK (1997) An elastic-viscous-plastic model for sea ice dynamics. J Phys Oceanogr 27:1849–1867

IPCC (2007) Climate Change 2007: the physical science basis. In: Solomon S, Qin D, Manning M, Chen Z, Marquis M, Averyt KB, Tignor M, Miller HL (eds) Contribution of Working Group I to the fourth assessment report of the Intergovernmental Panel on Climate Change. Cambridge University Press, Cambridge, 996 pp

Jochum M, Danabasoglu G, Holland M, Kwon YO, Large WG (2008) Ocean viscosity and climate. J Geophys Res 113. doi:10.1029/2007JC004515

Kauker F, Kaminski T, Karcher M, Giering R, Gerdes R, Voßbec M (2009) Adjoint analysis of the 2007 all time Arctic sea-ice minimum. Geophys Res Lett 36. doi:10.1029/2008GL036323

Kay JE, L'Ecuyer T, Gettleman A, Stephens G, O'Dell C (2008) The contribution of cloud and radiation anomalies to the 2007 Arctic sea ice extent minimum. Geophys Res Lett 35:L08503. doi:10.1029/2008GL033451

Koenigk T, Mikolajewicz U (2008) Seasonal to interannual climate predictability in mid and high northern latitudes in a global coupled model. Clim Dyn. doi:10.1007/s00382-008-0419-1

Large WG, McWilliams JC, Doney SC (1994) Ocean vertical mixing: a review and a model with a nonlocal boundary layer parameterization. Rev Geophys 32:363–403

Lindsay RW, Zhang J, Schweiger AJ, Steele MA (2008) Seasonal predictions of ice extent in the Arctic Ocean. J Geophys Res 113:C02023. doi:10.1029/2007JC004259

Lindsay RW, Zhang J, Schweiger A, Steele M, Stern H (2009) Arctic sea ice retreat in 2007 follows thinning trend. J Clim 22:165–176

Bitz CM, Lipscomb WH (1999) An energy-conserving thermodynamic model of sea ice. J Geophys Res 104:15669–15677

Lipscomb WH (2001) Remapping the thickness distribution in sea ice models. J Geophys Res 106(13):13989–14000

Maslanik JA, Fowler C, Stroeve J, Drobot S, Zwally J, Yi D, Emery W (2007) A younger, thinner Arctic ice cover: increased potential for rapid, extensive sea-ice loss. Geophys Res Lett 34:L24501. doi:10.1029/2007GL032043

Meehl GA et al (2006) Climate change projections for the twenty-first century and climate change commitment in the CCSM3. J Clim 19(11):2597–2616

Overland JE, Spillane MC, Soreide NN (2004) Integrated analysis of physical and biological pan-arctic change. Clim Change 63:291–322

Pohlmann H, Botzet M, Latif M, Roesch A, Wild M, Tschuck P (2004) Estimating the decadal predictability of a coupled AOGCM. J Clim 17:4463–4472

Rothrock DA, Zhang J, Yu Y (2003) The arctic ice thickness anomaly of the 1990s: a consistent view from observations and models. J Geophys Res 108(C3):3038 (28–37). doi:10.1029/2001JC001208

Schweiger AJ, Zhang J, Lindsay RW, Steele M (2008) Did unusually sunny skies help drive the record sea ice minimum of 2007? Geophys Res Lett 35:L10503. doi:10.1029/2008GL033463

Serreze MC, Holland MM, Stroeve J (2007) Perspectives on the Arctic's shrinking sea-ice cover. Science 315:1533–1536

Smith R, Gent P (2004) Reference manual for the Parallel Ocean Program (POP) ocean component of the Community Climate System Model (CCSM2.0 and 3.0). LAUR-02-2484. Los Alamos National Laboratory, Los Alamos

Stroeve JC, Holland MM, Meier W, Scambos T, Serreze MC (2007) Arctic sea ice decline: faster than forecast. Geophys Res Lett 34:L09501. doi:10.1029/2007GL029703

Stroeve J, Serreze M, Drobot S, Gearhead S, Holland M, Maslanik J, Meier W, Scambos T (2008) Arctic sea ice plummets in 2007. EOS 89(2):13–14

Thorndike AS, Rothrock DS, Maykut GA, Colony R (1975) Thickness distribution of sea ice. J Geophys Res 80:4501–4513

Walsh JE (1980) Empirical orthogonal functions and the statistical predictability of sea ice extent. In: Pritchard RS (ed) Sea ice processes and models. University of Washington Press, Seattle, pp 373–384

Zhang X, Walsh JE (2006) Toward a seasonally ice-covered Arctic Ocean: scenarios from the IPCC AR4 model simulations. J Clim 19:1730–1747

Zhang J, Steele M, Lindsay R, Schweiger A, Morison J (2008a) Ensemble 1-year predictions of Arctic sea ice for the spring and summer of 2008. Geophys Res Lett 35:L08502. doi:10.1029/2008GL033244

Zhang J, Lindsay R, Steele M, Schweiger A (2008b) What drove the dramatic retreat of Arctic sea ice during summer 2007? Geophys Res Lett 35:L11505. doi:10.1029/2008GL034005